

# TOMOGRAPHY OF THE SOLAR WIND USING INTERPLANETARY SCINTILLATIONS

A Thesis

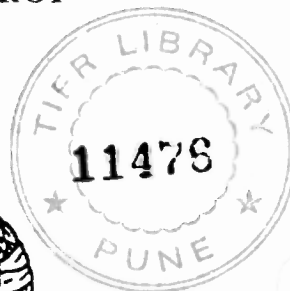
Submitted for the Degree of

**Doctor of Philosophy**

in the Faculty of Science

By

**DIVYA OBEROI**



NCRA LIBRARY



011476

Department of Physics

**INDIAN INSTITUTE OF SCIENCE**

BANGALORE-560 012, (INDIA)

JULY 2000

## DECLARATION

I hereby declare that the work presented in this thesis is entirely original, and it has been carried out by me at the National Centre for Radio Astrophysics, TIFR, Pune, under the auspices of the Joint Astronomy Programme of the Department of Physics, Indian Institute of Science, Bangalore. I further declare that this has not formed the basis of award of any degree, diploma, membership, associateship or similar title of any University or Institution.

Divya Oberoi

Department of Physics,  
Indian Institute of Science,  
Bangalore - 560 012,  
INDIA.

## Acknowledgements

It has been a rewarding experience to have worked with Pramesh, my thesis supervisor. I much appreciate the freedom which he allowed me all along, right from the choice of the problem to the manner in which it was addressed. I hope it has been an interesting experience for him as well.

I thank V. Balasubramainam for making the Ooty Radio Telescope available for my observations for almost five uninterrupted months and for providing his catalogue of scintillating sources. Thanks are due to P. K. Manoharan for providing information about several other sources which were included in the observations. I am much indebted to the observing and technical staff at Radio Astronomy Centre, Ooty, without whose dedication and support these observations would not have been possible. I thank all NCRA staff members for their help on numerous occasions.

It is a pleasure to acknowledge the illuminating and fruitful discussions with Rajaram, I only wish that I had interacted with him more. I wish to thank Chanda Jog and Arnab Rai Choudhuri for their willing help on various occasions.

This research would not have been possible without the extensive use of the large body of *free* software made available by the Free Software Foundation and other organisations and individuals, too numerous to name individually. I acknowledge the efforts and the spirit of the authors of the free software used and hope to join their ranks some day. This research has made use of NASA's Astrophysics Data System Abstract Service. Data from ULYSSES and WIND space missions used in this work have been obtained from the archives of National Space Science Data Center, a part of NASA. The SOHO/LASCO data used here are produced by a consortium of the Naval Research Laboratory (USA), Max-Planck-Institut fuer Aeronomie (Germany), Laboratoire d'Astronomie (France), and the University of Birmingham (UK). SOHO is a project of international cooperation between ESA and NASA.

The many friends I made during my stay at NCRA and IISc have enriched my life and are fondly remembered. I have learnt large amounts from Sanjay and Rajiv Singh about both software and larger things in life.

I thank my parents for their constant support, encouragement and understanding. I appreciate the patience of my wife, Jayshree, for tolerating me all through and even being enthusiastic about it. I sincerely appreciate the consideration shown by my daughter, who postponed her arrival to the day I finally finished writing my thesis.

## List of Publications

1. A. P. Rao, S. Ananthakrishnan, V. Balasubramanian, W. A. Coles and **D. Oberoi**, 1995 Very long baseline IPS observations of the Solar Wind speed in the fast polar streams, *Solar Wind 8*, AIP Conference Proceedings 382, 511-514, 1995.
2. **D. Oberoi** and A. P. Rao, 1999, Tomography of the Solar Wind using Interplanetary Scintillation, to appear in proceedings of the IAU Colloquium 179 on *Cyclic evolution of the Solar magnetic fields: advances in theory and observations*, December 1999.

## Synopsis

The Solar Wind is a neutral plasma which constantly flows out from the Sun and permeates the interplanetary space. The density inhomogeneities in this plasma cause the plane wavefront from a distant compact radio source to develop phase corrugations as it travels through it. By the time the corrugated wavefront travels to the observer, at the Earth, the phase corrugations develop into an interference pattern. The relative motion between the Solar Wind and the Earth causes this interference pattern to sweep past the telescope, translating the spatial variations of the interference pattern into temporal intensity scintillations. These intensity scintillations are referred to as Interplanetary Scintillations (IPS). Since its discovery in the mid sixties, IPS has been extensively used as a remote sensing technique to study a variety of aspects of the Solar Wind, ranging from the large scale properties of the *normal* Solar Wind and their changes with the solar cycle, to characterising the disturbances in the interplanetary medium due to transient activities on the Sun. IPS observations have also been used to estimate the angular sizes of the scintillating components in the observed sources.

Solar Wind has been studied using both direct observations by spacecrafts and observations using remote sensing techniques like IPS. The *in-situ* sampling of the Solar Wind by spacecrafts have the advantage that the physical properties of interest are often directly measurable and fewer assumptions are necessary for interpretation of the data. A limitation of spacecraft measurements is that they provide only spot measurements of the Solar Wind and the observations from a single spacecraft cannot distinguish between temporal and spatial variations in a model independent manner. IPS, on the other hand, is sensitive to a weighted sum of distribution of the properties of the Solar Wind along the *line-of-sight* and observations at meter wavelengths have a large fraction of the inner heliosphere accessible to them any given time. Most means of studying the Solar Wind observe either close to the solar disc or perform *in-situ* sampling in the ecliptic plane at 1 *AU*, while IPS can provide measurements in the intervening region from about 0.3 *AU* out to 1.0 *AU* and thus provides the missing link to relate the observations close to the Sun to the observations at 1 *AU*. The information which can be made available by IPS is not obtainable by any other means. The IPS measurables being *l.o.s.* integrals, it is not possible to reconstruct the distribution of the physical properties from measurements along individual *l.o.s.s* and this is the main limitation of IPS.

As IPS measurements carry an integrated information of the Solar Wind along the *l.o.s.* to the radio source, it is possible to get information of about the global structure of the Solar Wind in the entire inner heliosphere, if IPS measurements are made along a large number of *l.o.s.s*, distributed such that they sample the a large volume of the inner heliosphere adequately. There have been attempts to model

the distribution of Solar Wind properties on a fiducial spherical surface, concentric with the Sun. Rather than trying to “deconvolve” the effects of *l.o.s.* integration, these attempts use the *P*-point assumption to assign the measurements made towards different *l.o.s.s* to a fiducial surface. The only IPS work which attempts a detailed tomographic reconstruction of the distribution of the Solar Wind properties, incorporating the effect of *l.o.s.* integration is by the UCSD and STElab groups<sup>1</sup>.

This thesis is a detailed study of the problem of tomographic reconstruction of the 3D distribution of the properties of the Solar Wind in the inner heliosphere. A precise formulation of the problem as best fit model estimation ( $\chi^2$  minimisation) exercise is presented. As the nature of geometry of IPS observations is such that the equatorial belt of the Sun is most suited for attempting a tomographic reconstruction, we have limited our study to this region. A necessary assumption, on which the success of this exercise depends, is that there is no significant time evolution in the structure of the Solar Wind during the period required to sample the entire heliosphere. This assumption is most likely to be valid close to solar minima.

A data-set, suitable for attempting tomographic reconstruction of the Solar Wind in the inner heliosphere, was acquired using the Ooty Radio Telescope, India which operates at 327 MHz. The epoch of observation was from April 1997 to August 1997 and started less than a year after the minima of the 23<sup>rd</sup> solar activity cycle. The data-set comprised of 5,418 observations, including the calibrator and off-source scans, totals to about 1,500 hrs of telescope time and spans about 5 Carrington rotations. The *P*-points of most of the *l.o.s.s* observed lie in an equatorial belt on the Sun within  $\pm 20^\circ$ . The elongation of most of the observations lie in the range  $20^\circ$  to  $80^\circ$ . This data provides a set of good *S/N* observations with a comprehensive coverage of the equatorial Solar Wind.

As the volume of the data-set was large, it was considered necessary to automate the analysis. A software analysis procedure has been developed to estimate the best fit to the observed power spectra of intensity scintillations using spherically symmetric Solar Wind models. This procedure has been tested rigorously using simulated data and has been shown to work reliably. It offers an objective means of estimating the best fit models to observed data and eliminates the possibility of human errors and biases creeping in the analysis. This procedure formed an important part of the exercise of tomographic reconstruction and made it possible to perform a large number of simulations, since it relieved the astronomer of the drudgery of having to estimate the IPS model parameters for each of the observed power spectra individually.

---

<sup>1</sup>Jackson et. al, JGR, **103**, 12049-12067, 1998 Kojima et. al, JGR, **103**, 1981-1989, 1998 and Asai et. al JGR, **103**, 1991-2001, 1998

The methodology followed for tomographic reconstruction involved the following steps. Using the automated procedure, single station IPS velocity and  $C_n^2$  were estimated, for all the *l.o.s.s* observed in a Carrington rotation period. The other IPS Solar Wind model parameters were fixed to reasonable values - a value of 1 for *Axial Ratio* and 3 for  $\alpha$  was used, while no inner scale was used. These *l.o.s.s* were mapped back to a discretised fiducial surface using the IPS velocity estimated for each of them. Rather than mapping back the model parameters to only the *P*-points of the *l.o.s.s*, they were mapped back to a band, of width  $5^\circ$ , on the fiducial surface with a weight corresponding to the IPS *l.o.s.* weight function. A weighted average of the all the contributions to each of the elemental areas (pixels) on the fiducial surface was used as the initial guess for the tomographic reconstruction process. The distribution of velocity and  $C_n^2$  on the fiducial surface formed the free parameters for the  $\chi^2$  minimisation problem and the power spectra observed along the various *l.o.s.s* were the constraints. For each model of velocity and  $C_n^2$  on the fiducial surface, the distribution of velocity and  $C_n^2$  along each *l.o.s.* was obtained and the model power spectra corresponding to it were computed. The  $\chi^2$  was computed between these model power spectra and the observed spectra and summed over all the observations. The global  $\chi^2$  so obtained was minimised using the *Downhill simplex* algorithm<sup>2</sup> and the result of the minimisation was the desired reconstructed distribution of the Solar Wind properties.

In order to establish the convergence and stability of the  $\chi^2$  minimisation procedure and validate the software developed for the purpose, a large number of simulations were done. The simulated data (model power spectra) satisfied the assumptions (no time and radial evolution) used by the analysis procedure, sampled the heliosphere using the same geometry parameters as the observed *l.o.s.s* and had an appropriate amount of noise added to them, to reflect the measurement uncertainty in the power spectra. The simulations were able to reconstruct the assumed distribution of Solar Wind properties on the fiducial surface for a variety of models and led to the conclusion that our observed sampling of the heliosphere was sufficient to reconstruct the structure of the Solar Wind.

The tomographic reconstruction method developed was applied to three of the Carrington rotation periods (1922 - 1924) where the data-set had adequate coverage of the equatorial belt. A strong transient event, an earth directed CME, took place in one of them (1922), therefore this period does not satisfy the requirements of no or little time evolution. The data from other rotations led to reasonable looking solutions but the results were not convincing because the solutions were not stable to perturbations to the initial simplex. The different starting simplexes lead to different final results having comparable values for  $\chi^2$  but which bore little resemblance to one another. The fact that the  $\chi^2$  minimisation converged for the simulations and did not

---

<sup>2</sup>Nelder and Mead, *Computer Journal*, **7**, 308-313, 1965

converge for observations leads to the conclusion that there are some fundamental differences between the simulated and the observed power spectra. These differences were investigated and the possible reasons for the lack of stability of  $\chi^2$  minimisation have been discussed.

While computing the initial guesses for the tomographic reconstruction process, it was noticed that the Solar Wind velocity tends to vary with distance from the Sun. In order to study this trend, the entire data-set was divided into three equal bins in heliocentric distances to the  $P$ -points of the  $l.o.s.s.$  These bins correspond to  $P$ -point distance ranges of  $0.34 - 0.55 AU$ ,  $0.55 - 0.76 AU$  and  $0.76 - 0.98 AU$ . For each of these bins, the same procedure as was used to generate the initial guess for the tomographic reconstruction, was used to compute the distribution of velocities on the fiducial surface. This distribution was averaged over longitude to obtain an average latitudinal velocity profile for each of the bins. These profiles show that the velocity increases by almost  $200 km s^{-1}$  as one moves from the equatorial regions towards either of the poles in a span about  $20^\circ$ , an increase of more than 50% over the mean value at the equator. The three latitudinal profiles show a clear trend for an average deceleration of the equatorial Solar Wind ( $\pm 15^\circ$ ) as it propagates radially outwards. The value of minima of the profiles decreased by  $75 km s^{-1}$  in the range of  $0.34$  to  $0.98 AU$ . As this trend is an unexpected one, a careful analysis of the various possible biases and artifacts was carried out. The analysis shows the trend to be genuinely present in the data. Our interpretation of this observations is also presented.





# Contents

<b>1</b>	<b>Introduction</b>	<b>1</b>
1.1	Interplanetary Scintillations . . . . .	1
1.2	Motivation for this thesis . . . . .	3
1.3	The present work . . . . .	5
1.4	Solar Wind . . . . .	6
1.4.1	Early Developments . . . . .	6
1.4.2	Parker's model . . . . .	7
1.5	Means of studying the Solar Wind . . . . .	7
1.6	Properties of the Solar Wind . . . . .	9
1.7	Organisation of the thesis . . . . .	20
<b>2</b>	<b>Theory of IPS</b>	<b>23</b>
2.1	The geometry of IPS observations . . . . .	23
2.2	IPS observables . . . . .	30
2.3	Basic IPS scenario . . . . .	31
2.4	IPS assumptions . . . . .	34
2.5	Power spectrum of intensity fluctuations . . . . .	38
2.5.1	Power spectrum of intensity fluctuations for a thin screen . . . . .	39
2.5.2	The extended medium . . . . .	43
2.5.3	Effect of finite source size . . . . .	44
2.5.4	Effect of receiver bandwidth . . . . .	45
2.5.5	The final expression . . . . .	47
2.6	Effects of variation of model parameters . . . . .	47

<b>3</b>	<b>Motivation for Tomographic Analysis</b>	<b>57</b>
3.1	Introduction . . . . .	57
3.2	Modelling Solar Wind using IPS observations . . . . .	57
3.2.1	Featureless Solar Wind models . . . . .	58
3.2.2	The 'P' point approximation . . . . .	61
3.3	Earlier attempts . . . . .	61
3.4	Deviations from uniform Solar Wind models . . . . .	64
3.4.1	Latitudinal structure of the Solar Wind . . . . .	64
3.4.2	Radial evolution of Solar Wind . . . . .	64
3.4.3	Solar activity and IPDs . . . . .	65
3.5	Tomography . . . . .	65
3.5.1	Formulation of the problem . . . . .	66
3.5.2	Reconstruction . . . . .	66
3.5.3	Applications . . . . .	68
3.6	Tomography and IPS . . . . .	69
3.7	Tomography assumptions . . . . .	70
3.8	Limitation of IPS tomography . . . . .	73
3.9	Problems envisaged . . . . .	74
3.10	Other attempts at obtaining the 3D structure of Solar Wind . . . . .	75
3.10.1	Solar Corona . . . . .	76
<b>4</b>	<b>Observations and Data analysis</b>	<b>77</b>
4.1	Introduction . . . . .	77
4.2	The Ooty Radio Telescope . . . . .	77
4.3	IPS Observations . . . . .	80
4.4	The Data-set . . . . .	80
4.4.1	Epoch . . . . .	80
4.4.2	Source Selection . . . . .	81
4.4.3	Considerations for Tomographic Reconstruction . . . . .	82
4.4.4	$\epsilon$ coverage . . . . .	82
4.5	Data Analysis . . . . .	88
4.5.1	Data Flagging . . . . .	88

4.5.2	Flux calibration . . . . .	88
4.5.3	Obtaining the power spectra . . . . .	90
4.5.4	Estimating the uncertainty in the power spectrum . . . . .	92
4.5.5	Uniform statistical averaging of the power spectra . . . . .	98
4.5.6	Computing the scintillation index . . . . .	100
4.5.7	Estimating the uncertainty in scintillation index . . . . .	101
4.5.8	Computing $g$ values . . . . .	102
<b>5</b>	<b>Single station IPS modelling</b>	<b>105</b>
5.1	Need for automated estimation of the best fit IPS model . . . . .	105
5.2	Criterion for $\chi^2$ definition . . . . .	106
5.3	Automated IPS model fitting . . . . .	107
5.3.1	The Philosophy . . . . .	107
5.3.2	Definition of $\chi^2$ . . . . .	107
5.3.3	The algorithm . . . . .	109
5.3.4	The Thin Screen power spectrum database . . . . .	109
5.3.5	Model parameters . . . . .	112
5.3.6	Correction for the Earth's velocity . . . . .	113
5.3.7	Generality of the formalism . . . . .	113
5.4	The simulations . . . . .	113
5.5	The results . . . . .	116
5.6	Reliability of the best fit IPS models . . . . .	119
5.7	A sample of the data . . . . .	134
5.8	Possible studies of the Solar Wind using the data-set . . . . .	149
<b>6</b>	<b>Radial Evolution of the Solar Wind</b>	<b>153</b>
6.1	Introduction . . . . .	153
6.2	Single station velocity determination . . . . .	154
6.3	The latitudinal profile of Solar Wind velocity . . . . .	155
6.4	The P-point approximation and its extension . . . . .	158
6.5	Discussion of possible artifacts and biases . . . . .	166
6.5.1	Artifacts due to sampling of the inner heliosphere . . . . .	166

6.5.2	Incorrect choices for Solar Wind model parameters . . . . .	170
6.5.3	Inadequacies of the IPS Solar Wind model . . . . .	172
6.5.4	Biases due to Signal to Noise problems . . . . .	172
6.6	Comparison with data from WIND . . . . .	173
6.6.1	Differences in sampling of the Solar Wind . . . . .	173
6.6.2	Heliographic latitude excursions of WIND . . . . .	175
6.6.3	Normalisation . . . . .	175
6.7	Comparison of WIND and ULYSSES data . . . . .	176
6.8	Conclusions . . . . .	181
<b>7</b>	<b>Tomographic Reconstruction Methodology</b> . . . . .	<b>185</b>
7.1	Introduction . . . . .	185
7.2	Methodology . . . . .	186
7.2.1	Formulation of the problem . . . . .	186
7.2.2	Generating the initial model . . . . .	189
7.2.3	Resolution : Constraints vs $\chi^2$ degrees of freedom . . . . .	189
7.2.4	The $\chi^2$ minimisation algorithm . . . . .	192
7.3	Coverage of the solar surface . . . . .	193
7.4	Software Issues . . . . .	196
7.5	Simulations . . . . .	196
7.5.1	Aim of the simulations . . . . .	197
7.5.2	Methodology . . . . .	197
7.6	Results of simulations . . . . .	199
7.6.1	Featureless Solar Wind models . . . . .	199
7.6.2	Solar Wind models with features . . . . .	202
7.7	Results from data . . . . .	231
7.8	Discussion . . . . .	252
7.9	Comparison with others similar exercises . . . . .	259
7.10	Possible improvements . . . . .	262
<b>8</b>	<b>Conclusions</b> . . . . .	<b>265</b>
8.1	Tomographic reconstruction of the Solar Wind . . . . .	265

8.1.1	Formulation of the problem . . . . .	265
8.1.2	Simulations . . . . .	266
8.2	Observations and analysis . . . . .	266
8.2.1	The data-set . . . . .	266
8.2.2	Automated best fit uniform Solar Wind model estimation . . .	267
8.2.3	Results of tomographic reconstruction . . . . .	267
8.3	Radial evolution of Solar Wind . . . . .	268
8.4	Future prospects of IPS tomography . . . . .	269
8.4.1	Need for better S/N observations . . . . .	269
8.4.2	Tomography as a routine investigation tool . . . . .	269
	Appendix A - Geometry of the Projection Region . . . . .	27
	The geometry of the projection region as seen by Solar Wind plasma at 1 AU . . .	27
2.1	The Sun, the Earth and the observational geometry . . . . .	27
2.2	The geometric projection of the line-of-sight on the solar surface . . . . .	28
2.3	Change in the heliographic latitude of the P-point with elongation . . . . .	29
2.4	Behaviour of the geometrically projected footpoints of the lines of sight with elongation . . . . .	30
2.5	Projected L.O.S. with propagation delay accounted for . . . . .	31
2.6	The transverse geometry . . . . .	35
2.7	The $m$ -curve . . . . .	36
2.8	The Pseud-Ring . . . . .	41
2.9	The thin screens along a L.O.S. . . . .	45
2.10	Effect of velocity of the Solar Wind on the power spectrum . . . . .	48
2.11	Effect of variation in $C_0$ on the power spectrum . . . . .	51
2.12	Effect of variation in size of the observed source on the power spectrum . . . . .	50
2.13	Effect of variation in Axial Ratio on the power spectrum . . . . .	52
2.14	Effect of variation in $\alpha$ on the power spectrum . . . . .	53
3.1	The component of velocity of Solar Wind perpendicular to the L.O.S. . . . .	59
3.2	The variation of $(\delta n)^2$ along the L.O.S. . . . .	61
3.3	Obtaining projection data for a tomographic reconstruction . . . . .	67

285  
286  
287  
288  
289  
290  
291  
292  
293  
294  
295  
296  
297  
298  
299  
300  
301  
302  
303  
304  
305  
306  
307  
308  
309  
310  
311  
312  
313  
314  
315  
316  
317  
318  
319  
320  
321  
322  
323  
324  
325  
326  
327  
328  
329  
330  
331  
332  
333  
334  
335  
336  
337  
338  
339  
340  
341  
342  
343  
344  
345  
346  
347  
348  
349  
350  
351  
352  
353  
354  
355  
356  
357  
358  
359  
360  
361  
362  
363  
364  
365  
366  
367  
368  
369  
370  
371  
372  
373  
374  
375  
376  
377  
378  
379  
380  
381  
382  
383  
384  
385  
386  
387  
388  
389  
390  
391  
392  
393  
394  
395  
396  
397  
398  
399  
400  
401  
402  
403  
404  
405  
406  
407  
408  
409  
410  
411  
412  
413  
414  
415  
416  
417  
418  
419  
420  
421  
422  
423  
424  
425  
426  
427  
428  
429  
430  
431  
432  
433  
434  
435  
436  
437  
438  
439  
440  
441  
442  
443  
444  
445  
446  
447  
448  
449  
450  
451  
452  
453  
454  
455  
456  
457  
458  
459  
460  
461  
462  
463  
464  
465  
466  
467  
468  
469  
470  
471  
472  
473  
474  
475  
476  
477  
478  
479  
480  
481  
482  
483  
484  
485  
486  
487  
488  
489  
490  
491  
492  
493  
494  
495  
496  
497  
498  
499  
500

*[Faint, illegible text representing the main content of the table of contents, including chapter titles and page numbers.]*

# List of Figures

1.1	The origin of Interplanetary Scintillations . . . . .	2
1.2	Speed of the Solar Wind with heliocentric distance . . . . .	8
1.3	Structure of the magnetic field in the Interplanetary Medium . . . . .	12
1.4	Formation of Co-rotating Interaction Regions . . . . .	15
1.5	An Interplanetary Disturbance, as seen in Solar Wind plasma at 1 AU	17
2.1	The Sun, the Earth and the line-of-sight geometry . . . . .	24
2.2	The geometric projection of the line-of-sight on the solar surface . . . . .	26
2.3	Change in the heliographic latitude of the P-point with elongation . . . . .	27
2.4	Behaviour of the geometrically projected footpoints of the lines-of-sight with elongation . . . . .	28
2.5	Projected <i>l.o.s.</i> with propagation delay accounted for . . . . .	29
2.6	The basic IPS geometry . . . . .	33
2.7	The m-p curve . . . . .	36
2.8	The Fresnel filter . . . . .	41
2.9	The thin screens along a <i>l.o.s.</i> . . . . .	43
2.10	Effect of velocity of the Solar Wind on the power spectrum . . . . .	48
2.11	Effect of variation in $C_n^2$ on the power spectrum . . . . .	49
2.12	Effect of variation in size of the observed source on the power spectrum	50
2.13	Effect of variation in Axial Ratio on the power spectrum . . . . .	52
2.14	Effect of variation in $\alpha$ on the power spectrum . . . . .	53
3.1	The component of velocity of Solar Wind perpendicular to the <i>l.o.s.</i> . . . . .	59
3.2	The variation of $(\delta n_e^2)^2$ along the <i>l.o.s.</i> . . . . .	60
3.3	Obtaining projection data for a tomographic reconstruction . . . . .	67

3.4	Heliospheric coverage of IPS observations . . . . .	71
3.5	Overlap of regions sampled by the IPS <i>l.o.s.s</i> . . . . .	72
4.1	The Ooty Radio Telescope . . . . .	78
4.2	Sunspot number progression for Solar cycle 23 . . . . .	81
4.3	Distribution of heliographic latitudes of the of observed sources . . . . .	85
4.4	Distribution of elongations of the observed sources . . . . .	86
4.5	Number of scans per day . . . . .	87
4.6	Counts/Jansky, $\xi$ , for the period of observations . . . . .	89
4.7	The power spectrum before and after correction for RC time constant and running mean subtraction . . . . .	91
4.8	An 'On-source' power spectrum . . . . .	93
4.9	An 'Off-source' power spectrum . . . . .	94
4.10	Subtraction of system noise from the power spectrum . . . . .	95
4.11	Percentage uncertainty in area under the power spectrum . . . . .	97
4.12	Distribution of uncertainty in area under the power spectrum . . . . .	97
4.13	Uniform statistically averaged power spectrum . . . . .	99
5.1	Distribution of $\chi^2$ for simulated data . . . . .	115
5.2	Distribution of $\chi^2$ . . . . .	117
5.3	$\chi^2$ as a function of percentage error on area under the power spectrum	118
5.4	IPS best fit models for $\chi^2 < 0.1$ and $A_{P(\nu)} < 1.0$ . . . . .	120
5.5	IPS best fit models for $\chi^2 < 0.1$ and $0.1 \leq A_{P(\nu)} < 10.0$ . . . . .	121
5.6	IPS best fit models for $0.1 \leq \chi^2 < 1.0$ and $A_{P(\nu)} < 1.0$ . . . . .	122
5.7	IPS best fit models for $0.1 \leq \chi^2 < 1.0$ and $0.1 \leq A_{P(\nu)} < 10.0$ . . . . .	123
5.8	IPS best fit models for $0.1 \leq \chi^2 < 1.0$ and $A_{P(\nu)} > 10.0$ . . . . .	124
5.9	IPS best fit models for $\chi^2 > 1.0$ and $A_{P(\nu)} < 1.0$ . . . . .	125
5.10	IPS best fit models for $\chi^2 > 1.0$ and $0.1 \leq A_{P(\nu)} < 10.0$ . . . . .	126
5.11	IPS best fit models for $\chi^2 > 1.0$ and $A_{P(\nu)} > 10.0$ . . . . .	127
5.12	Power spectra with the largest $\chi^2$ . . . . .	128
5.13	Power spectra with the largest velocities . . . . .	130
5.14	Power spectra with the smallest velocities . . . . .	131



5.15	Power spectra with the highest $g$ values . . . . .	132
5.16	Power spectra with the lowest $g$ values . . . . .	133
5.17	Observations of 0518+165 . . . . .	135
5.18	Observations of 0725+147 . . . . .	136
5.19	Observations of 0005-062 . . . . .	137
5.20	Observations of 0202+149 . . . . .	138
5.21	Observations of 0316+162 . . . . .	139
5.22	Observations of 0116+082 . . . . .	140
5.23	Observations of 0531+194 . . . . .	141
5.24	Observations of 0758+143 . . . . .	142
5.25	Observations of 0316+413 . . . . .	143
5.26	Observations of 0459+252 . . . . .	144
5.27	Observations of 0548+165 . . . . .	145
5.28	Observations of 0349+063 . . . . .	146
5.29	Observations of 2322-052 . . . . .	147
6.1	Average velocity structure of the Solar Wind along heliographic latitude	157
6.2	The results of the $P$ -point analysis . . . . .	159
6.3	Line-of-sight weight threshold of 0.50 . . . . .	160
6.4	Line-of-sight weight threshold of 0.05 . . . . .	161
6.5	Line-of-sight weight threshold of 0.50 and a width of $5^\circ$ . . . . .	162
6.6	Smoothed $P$ -point latitudinal velocity profiles: Bin 1 and 2 . . . . .	164
6.7	Smoothed $P$ -point latitudinal velocity profiles: Bin 3 . . . . .	165
6.8	The distributions of $P$ -points . . . . .	167
6.9	Latitudinal velocity profiles for simulated data . . . . .	169
6.10	Heliographic coordinates of WIND . . . . .	174
6.11	The relative locations of ULYSSES and WIND . . . . .	178
6.12	The trajectory of ULYSSES and WIND spacecrafts . . . . .	179
6.13	Variation in Solar Wind velocity with heliocentric distance . . . . .	180
6.14	Solar Wind velocity measured by WIND . . . . .	183
7.1	The flow chart for the tomographic reconstruction process . . . . .	190

7.2	Solar surface coverage for Carrington rotations 1922 and 1923 . . . . .	194
7.3	Solar surface coverage for Carrington rotations 1924 and 1925 . . . . .	195
7.4	Velocity vs $\chi^2$ : Solar Wind model D . . . . .	204
7.5	Velocity and $\chi^2$ histograms : Solar Wind model D . . . . .	205
7.6	Velocity reconstruction for model D (noisefree data) . . . . .	207
7.7	$C_n^2$ reconstruction for model D (noisefree data) . . . . .	208
7.8	Reduction in $\chi_G^2$ for model D . . . . .	210
7.9	Assessing the quality of the tomographic reconstruction . . . . .	212
7.10	Comparison of $\chi^2$ from tomographic reconstruction and uniform Solar Wind models . . . . .	213
7.11	Velocity reconstruction for model D (noise added data) . . . . .	215
7.12	$C_n^2$ reconstruction for model D (noise added data) . . . . .	216
7.13	Velocity reconstruction for model E1 . . . . .	218
7.14	$C_n^2$ reconstruction for model E1 . . . . .	219
7.15	Velocity reconstruction for model E2 . . . . .	220
7.16	$C_n^2$ reconstruction for model E2 . . . . .	221
7.17	Velocity reconstruction for model E3 . . . . .	222
7.18	$C_n^2$ reconstruction for model E3 . . . . .	223
7.19	Velocity reconstruction for model F1 . . . . .	226
7.20	$C_n^2$ reconstruction for model F1 . . . . .	227
7.21	Velocity reconstruction for model F2 . . . . .	228
7.22	$C_n^2$ reconstruction for model F2 . . . . .	229
7.23	Velocity reconstruction for Carrington rotation 1923 . . . . .	233
7.24	$C_n^2$ reconstruction for Carrington rotation 1923 . . . . .	234
7.25	Reduction in $\chi_G^2$ achieved by tomographic reconstruction for Carring- ton rotation 1923 . . . . .	235
7.26	Some more velocity reconstructions for Carrington Rotation 1923 . . . . .	236
7.27	Some more $C_n^2$ reconstructions for Carrington Rotation 1923 . . . . .	237
7.28	LASCO Synoptic map for Carrington rotation 1923 . . . . .	239
7.29	Solar Wind velocity measured by WIND . . . . .	240
7.30	Velocity reconstruction for Carrington rotation 1922 . . . . .	241
7.31	$C_n^2$ reconstruction for Carrington rotation 1922 . . . . .	242

7.32	LASCO Synoptic map for Carrington rotation 1922 . . . . .	243
7.33	Velocity reconstruction for Carrington rotation 1924 . . . . .	245
7.34	$C_n^2$ reconstruction for Carrington rotation 1924 . . . . .	246
7.35	LASCO Synoptic map for Carrington rotation 1924 . . . . .	247
7.36	Velocity reconstruction for Carrington rotation 1925 . . . . .	248
7.37	$C_n^2$ reconstruction for Carrington rotation 1925 . . . . .	249
7.38	LASCO Synoptic map for Carrington rotation 1925 . . . . .	250
7.39	The density of coverage for Carrington rotations 1922–1925 . . . . .	251
7.40	Contributions to a pixel on the fiducial surface – 1 . . . . .	254
7.41	Contributions to a pixel on the fiducial surface – 2 . . . . .	255
7.42	Contributions to a pixel on the fiducial surface – 3 . . . . .	256
7.43	$\chi_G^2$ landscape . . . . .	258

215	7.27	SAFAR Wind velocity measured by WIND	240
216	7.28	JASCO Synoptic map for Caribbean rotation 1923	241
217	7.29	Some more $C_2^2$ reconstructions for Caribbean Rotation 1923	247
218	7.30	Some more velocity reconstructions for Caribbean Rotation 1923	248
219	7.31	Reduction in $\chi^2$ achieved by tomographic reconstruction for Caribbean rotation 1923	253
220	7.32	$C_2^2$ reconstruction for Caribbean rotation 1923	254
221	7.33	Velocity reconstruction for Caribbean rotation 1923	255
222	7.34	SAFAR Wind velocity measured by WIND	240
223	7.35	JASCO Synoptic map for Caribbean rotation 1923	241
224	7.36	Some more $C_2^2$ reconstructions for Caribbean Rotation 1923	247
225	7.37	Some more velocity reconstructions for Caribbean Rotation 1923	248
226	7.38	Reduction in $\chi^2$ achieved by tomographic reconstruction for Caribbean rotation 1923	253
227	7.39	$C_2^2$ reconstruction for Caribbean rotation 1923	254
228	7.40	Velocity reconstruction for Caribbean rotation 1923	255
229	7.41	Contributions to a pixel on the fiducial surface - 1	261
230	7.42	Contributions to a pixel on the fiducial surface - 2	262
231	7.43	Contributions to a pixel on the fiducial surface - 3	263
232	7.44	Contributions to a pixel on the fiducial surface - 4	264
233	7.45	Contributions to a pixel on the fiducial surface - 5	265
234	7.46	Contributions to a pixel on the fiducial surface - 6	266
235	7.47	Contributions to a pixel on the fiducial surface - 7	267
236	7.48	Contributions to a pixel on the fiducial surface - 8	268
237	7.49	Contributions to a pixel on the fiducial surface - 9	269
238	7.50	Contributions to a pixel on the fiducial surface - 10	270
239	7.51	Contributions to a pixel on the fiducial surface - 11	271
240	7.52	Contributions to a pixel on the fiducial surface - 12	272
241	7.53	Contributions to a pixel on the fiducial surface - 13	273
242	7.54	Contributions to a pixel on the fiducial surface - 14	274
243	7.55	Contributions to a pixel on the fiducial surface - 15	275
244	7.56	Contributions to a pixel on the fiducial surface - 16	276
245	7.57	Contributions to a pixel on the fiducial surface - 17	277
246	7.58	Contributions to a pixel on the fiducial surface - 18	278
247	7.59	Contributions to a pixel on the fiducial surface - 19	279
248	7.60	Contributions to a pixel on the fiducial surface - 20	280
249	7.61	Contributions to a pixel on the fiducial surface - 21	281
250	7.62	Contributions to a pixel on the fiducial surface - 22	282
251	7.63	Contributions to a pixel on the fiducial surface - 23	283
252	7.64	Contributions to a pixel on the fiducial surface - 24	284
253	7.65	Contributions to a pixel on the fiducial surface - 25	285
254	7.66	Contributions to a pixel on the fiducial surface - 26	286
255	7.67	Contributions to a pixel on the fiducial surface - 27	287
256	7.68	Contributions to a pixel on the fiducial surface - 28	288
257	7.69	Contributions to a pixel on the fiducial surface - 29	289
258	7.70	Contributions to a pixel on the fiducial surface - 30	290
259	7.71	Contributions to a pixel on the fiducial surface - 31	291
260	7.72	Contributions to a pixel on the fiducial surface - 32	292
261	7.73	Contributions to a pixel on the fiducial surface - 33	293
262	7.74	Contributions to a pixel on the fiducial surface - 34	294
263	7.75	Contributions to a pixel on the fiducial surface - 35	295
264	7.76	Contributions to a pixel on the fiducial surface - 36	296
265	7.77	Contributions to a pixel on the fiducial surface - 37	297
266	7.78	Contributions to a pixel on the fiducial surface - 38	298
267	7.79	Contributions to a pixel on the fiducial surface - 39	299
268	7.80	Contributions to a pixel on the fiducial surface - 40	300
269	7.81	Contributions to a pixel on the fiducial surface - 41	301
270	7.82	Contributions to a pixel on the fiducial surface - 42	302
271	7.83	Contributions to a pixel on the fiducial surface - 43	303
272	7.84	Contributions to a pixel on the fiducial surface - 44	304
273	7.85	Contributions to a pixel on the fiducial surface - 45	305
274	7.86	Contributions to a pixel on the fiducial surface - 46	306
275	7.87	Contributions to a pixel on the fiducial surface - 47	307
276	7.88	Contributions to a pixel on the fiducial surface - 48	308
277	7.89	Contributions to a pixel on the fiducial surface - 49	309
278	7.90	Contributions to a pixel on the fiducial surface - 50	310
279	7.91	Contributions to a pixel on the fiducial surface - 51	311
280	7.92	Contributions to a pixel on the fiducial surface - 52	312
281	7.93	Contributions to a pixel on the fiducial surface - 53	313
282	7.94	Contributions to a pixel on the fiducial surface - 54	314
283	7.95	Contributions to a pixel on the fiducial surface - 55	315
284	7.96	Contributions to a pixel on the fiducial surface - 56	316
285	7.97	Contributions to a pixel on the fiducial surface - 57	317
286	7.98	Contributions to a pixel on the fiducial surface - 58	318
287	7.99	Contributions to a pixel on the fiducial surface - 59	319
288	7.100	Contributions to a pixel on the fiducial surface - 60	320

# List of Tables

1.1	Statistical properties of the Solar Wind at 1 AU in the ecliptic plane	19
4.1	List of sources observed	83
5.1	IPS model parameters available in the thin screen spectra database	110
5.2	Results of automated IPS model estimation simulations	114
6.1	Elongation and $P$ -point distance bins	155
7.1	Global Solar Wind model $\chi^2$ minimisation : Featureless models	200
7.2	Distribution of constraints : Model D	209
7.3	Global Solar Wind model $\chi^2$ minimisation : Models with two features	224

List of Tables

1.1 Statistical properties of the Solar Wind at 1 AU in the ecliptic plane 19

4.1 List of sources observed 33

5.1 IFS model parameters available in the thin screen spectra database 110

6.2 Results of numerical IFS model estimation simulations 114

6.1 Estimation and  $\chi^2$ -point distance plots 155

7.1 Global Solar Wind model  $\chi^2$  minimization: Parameter models 200

7.2 Distribution of constraints: Model D 209

7.3 Global Solar Wind model  $\chi^2$  minimization: Models with two latitudes 224

# Chapter 1

## Introduction

### 1.1 Interplanetary Scintillations

The Solar Wind is a neutral plasma which constantly flows out from the Sun and permeates the interplanetary space. The density inhomogeneities in this plasma cause the plane wavefront from a distant compact radio source to develop phase corrugations as it travels through it. By the time the corrugated wavefront travels to the plane of observation, at the Earth, the phase corrugations develop into an interference pattern. The scenario is shown schematically in figure 1.1. The motion of the Solar Wind causes this interference pattern to sweep past the telescope, translating the spatial variations of the interference pattern into temporal intensity scintillations. These intensity scintillations are referred to as Interplanetary Scintillations (IPS). This phenomenon finds a good analogy in the twinkling of stars due to turbulence in the atmosphere.

Hewish, Scott and Wills (Hewish et al., 1964) are credited with the discovery of this phenomenon and offering the explanation for its cause. Since its discovery in the mid sixties, IPS has been extensively used as a remote sensing technique to study the Solar Wind. IPS has been used to study a variety of aspects of the Solar Wind ranging from the large scale properties of the *normal* Solar Wind to characterising the disturbances in the interplanetary medium due to transient activities on the Sun. Considerable information about the global structure of the Solar Wind and its changes with solar cycle has been obtained using IPS studies. Physical parameters of the interplanetary disturbances and their associations with events on the Sun have also been an active area of research. An excellent review of the work done in the pre 1978 period is provided by Coles (Coles, 1978). A more recent review by Kojima and Kakinuma (Kojima and Kakinuma, 1990) incorporates almost all major developments and focuses mainly on studies of global structure and solar cycle dependence of the Solar Wind, as learnt from IPS observations.

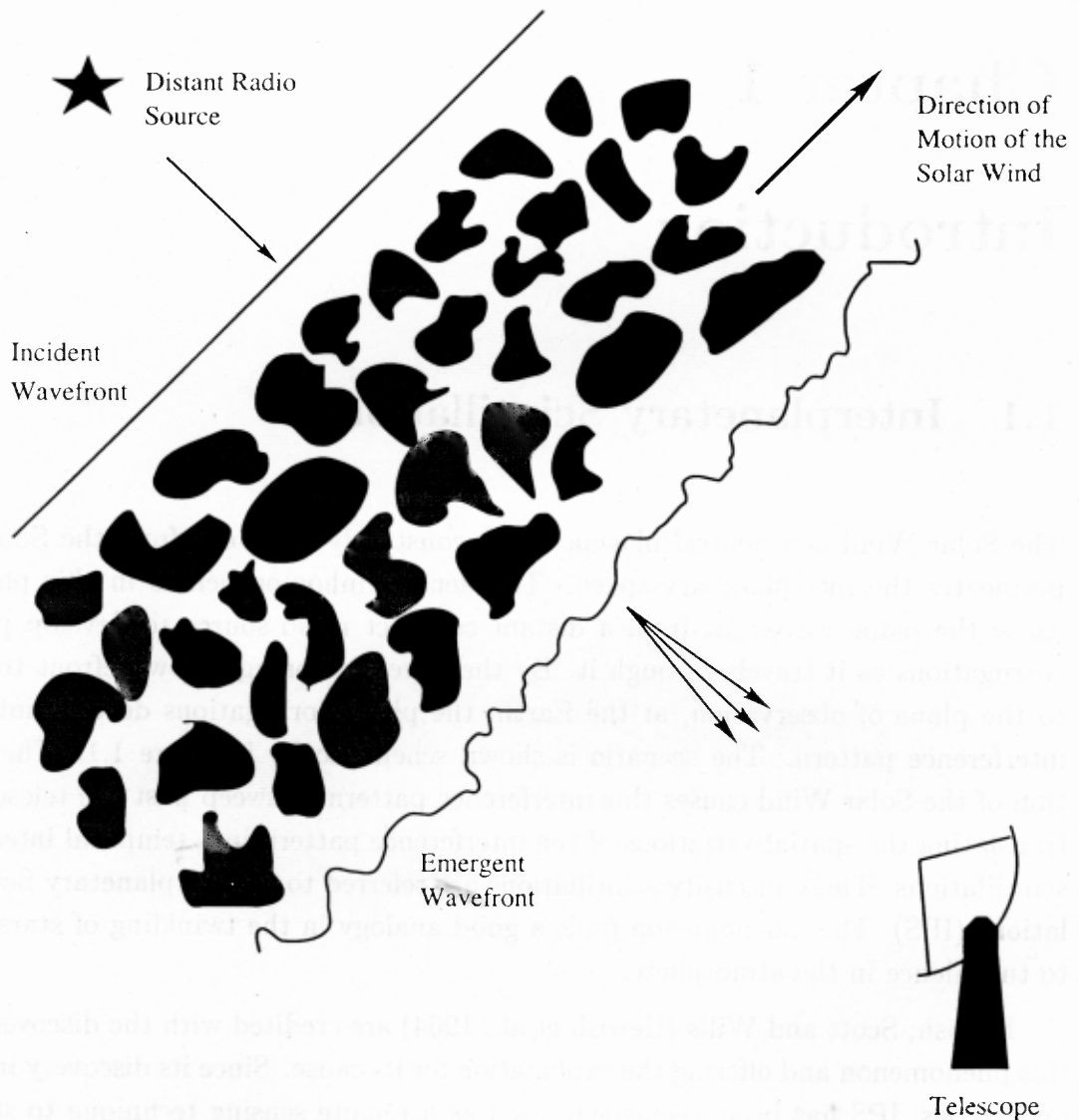


Figure 1.1: **The origin of Interplanetary Scintillations - A schematic illustration** – The Solar Wind acts as a medium with fluctuating refractive index to the incident plane wavefront from a distance radio source. The emergent wavefront carries an imprint of these fluctuations as phase corrugations which develop into an interference pattern by the time it arrives at the observing plane. The motion of the Solar Wind causes this interference pattern to sweep past the telescope giving rise to Interplanetary Scintillations.



The intensity scintillations also depend on the structure of the scintillating source. There have, therefore, been many studies which have used IPS to try to unravel the structure the source, assuming average properties for the Solar Wind. Before the advent of Very Long Baseline Interferometry (VLBI), IPS and Lunar occultation studies were the only means of obtaining sub arc second resolutions. An added advantage which stands even today is that IPS gives high resolution information at low frequencies where rather few VLBI studies have been undertaken. Major surveys were undertaken by Little and Hewish (Little and Hewish, 1968) at 178  $MHz$ , Cohen (Cohen et al., 1968) at 430  $MHz$  and Bhandari et. al. (Bhandari et al., 1974) at 327  $MHz$  which derived the structures of the scintillating sources in late 1960s and early 1970s.

A large number of instruments, both ground and space based, are dedicated to study the solar disc and the corona over a large range of the electromagnetic spectrum. The many Earth orbiting satellites at 1  $AU$ <sup>1</sup> measure various physical properties of the local Solar Wind. IPS provides measurements of the Solar Wind in the intervening region from about 0.1  $AU$  out to 1.0  $AU$  and thus provide the missing link to allow the observations close to the Sun to be related to the Solar Wind observed at 1  $AU$ . These observations can also help in studying the evolution of the Solar Wind plasma as it travels out from the Sun.

## 1.2 Motivation for this thesis

IPS measurements carry an integrated information of the Solar Wind along the *line-of-sight* (*l.o.s.*) to the radio source. It is conceptually simple to realise that if IPS measurements are made along a large number of *l.o.s.*s distributed such that they sample a large volume of the heliosphere adequately, such a data-set must have the information of the global structure of the Solar Wind in the entire inner heliosphere hidden in it. The problem of extracting this information from the data-set is conceptually similar to that of *tomography*, where one tries to reconstruct the structure of a  $N$  dimensional object from its projections in  $N - 1$  dimensions.

The proposition of reconstructing the global structure of Solar Wind using IPS is aided by the following facts - IPS can sample a large fraction of the heliosphere at any given time and the rotation of the Sun presents many different perspectives of the same physical regions of the heliosphere to the observer. The epoch of observation available to us was close to the solar minima, this is the epoch when the time evolution of the features on the Sun is expected to be the least. The fact that Solar Wind can be modelled well by a purely radial outflow with a constant velocity allows one to make a simple model for propagation of the Solar Wind. Most attempts at

---

<sup>1</sup>1  $AU = 1.49 \times 10^8$  km

modelling the Solar Wind, in the past, implicitly assume it to have a relatively simple structure which can be represented adequately with a few features.

If one is able to achieve a reliable reconstruction of the Solar Wind in the inner heliosphere, there are a fair number of issues on which such the results of such an exercise can shed light. The most important among these are :

1. The radial evolution of the Solar Wind as it traverses out from close to the Sun to 1 *AU* is still poorly studied, mainly because of the lack of a suitable data-set. These observations can provide a data-set suitable for such studies.
2. Close to the solar minima, well defined and stable Co-rotating Interaction Regions (CIRs) are formed near the solar equator. The CIRs are usually detected in the plasma data obtained from satellites at 1 *AU* or beyond and are correlated with the locations of the coronal holes on the solar disc. Their evolution and properties are yet to studied in significant detail in the inner heliosphere. A study which can be made possible by this data-set.
3. IPS is sensitive to the level of turbulence in the Solar Wind. Correlations with other synoptic observations is expected to lead to some information about the features on the solar disc which contribute significant turbulence in the Solar Wind.
4. As the data-set will span a large duration, it is very likely that some transient events take place during the course of the observations. As the observing strategy would be optimised to get the best possible coverage of the heliosphere, the interplanetary disturbance will also be very well sampled along an entire range of heliospheric distances. Data-sets with such extensive coverage of transients can yield comparatively well constrained models for the disturbance and its evolution with heliospheric distances.

Such a detailed study using the IPS data may lead to some surprises as well, as most of the data-sets available in the past have usually been too sparse to look for fine features.

A data-set suitable for such an exercise shall necessarily require large amounts of observing time on a sensitive telescope, in order to achieve a good coverage of the heliosphere. We had our disposal practically unlimited observing time at the *Ooty Radio Telescope*, which is a very sensitive instrument for this exercise. This exercise provided a good opportunity to exploiting this advantage to the hilt.

### 1.3 The present work

It was argued in the previous section that IPS observations can generate a data-set which has the information of the global structure of the Solar Wind in the entire inner heliosphere. The reconstruction of the global structure of the Solar Wind from such data relies crucially on the assumption that the time evolution, in the minimum duration of the period which is required to obtain a complete coverage of the heliosphere, is not significant enough to render the data-set inconsistent. Other, equally crucial, inputs to the reconstruction process are the laws of propagation of the Solar Wind. The most important aspects which have been dealt with in the present work are enumerated below :

1. The starting point of this exercise was to acquire an IPS data-set which is suited to the requirements of attempting a tomographic reconstruction of the Solar Wind in the inner heliosphere. Such a data-set has been obtained using the Ooty Radio Telescope, India. The data-set has extensive coverage of the relevant parts of the inner heliosphere, spans more than 4 Carrington rotations, amounts to 5, 418 observations of scintillating sources and calibrators and used  $\sim 1, 500$  hrs of telescope time. This data-set is one of the few of its kind which provide a dense coverage of the inner heliosphere for extended periods of time.
2. An automated procedure to estimate the parameters of the featureless Solar Wind model which represent the best fit to the observed data has been developed. The procedure has been tested rigorously and has been demonstrated to work efficiently. This procedure provides, for the first time, an objective means of arriving at the parameters of best fit featureless Solar Wind model. The availability of such a procedure reduces the possibilities of human errors and biases and also the drudgery involved in fitting models to large volumes of data. It forms an important part of the tomographic reconstruction procedure and has made it possible to run many more simulations and experiments than would have been possible otherwise.
3. It was required to develop an analysis procedure which uses the IPS data as input and provides a global model for 3D distribution of the physical properties of the Solar Wind consistent with the data-set as the output. An analysis procedure which fulfils these requirements has been developed. This procedure has been extensively tested using simulated data which satisfies the assumption of no time and radial evolution made by the analysis procedure. It has been established that the analysis procedure is sensitive to stable structures in the Solar Wind and the coverage of the heliosphere obtained by the data-set is adequate to reconstruct the structure of the Solar Wind in the equatorial belt of the Sun.

4. Having ascertained the effectiveness of the reconstruction procedure on simulated data, it was next required to establish if the assumptions required by the procedure are met by the IPS data obtained. The effects of violations of the assumptions and the reliability of the tomographically reconstructed models for the Solar Wind in the inner heliosphere have been studied.
5. The data-set obtained being very well suited for studying the radial evolution of the Solar Wind properties, we performed a careful analysis to study the radial evolution of the average velocity of the Solar Wind. This exercise led to the conclusion that the average IPS velocity of the Solar Wind shows a trend to decrease slightly between 0.3 and 1  $AU$ . This conclusion is at variance with the standard models for the Solar Wind which predict the velocity to increase slightly in the range of the radial distances studied. We present an explanation for the trend seen in the data.

Any transient events on the Sun during the course of the observations which give rise to disturbances which propagate through the Interplanetary Medium are quite likely to be sampled very well by the data-set. The data corresponding to the events can be used independently to build a detailed model for the Interplanetary Disturbances. Two significant transient events which led to Interplanetary Disturbances (Section 1.6) took place during the period of the observations and have both been very well sampled by the data-set.

## 1.4 Solar Wind

### 1.4.1 Early Developments

The earliest hints about events on the Sun having a significant effect on the Earth came about 150 years ago. Carrington, in 1859, noticed that a major geomagnetic storm began about 1.5 days after a solar flare was observed on the Sun. He tentatively suggested a causal relationship between the solar and geomagnetic events. Subsequent investigations revealed numerous examples of apparent associations between solar flares and large geomagnetic storms. Lindemann tried to explain this relationship by suggesting that the geomagnetic storms result from an interaction between the geomagnetic field and the high speed plasma ejected into the Interplanetary Space by solar activity. A periodicity of 27 days, the rotation period of the Sun as observed from Earth, was also noticed fairly early in the studies of geomagnetic activity. The persistent presence of some form of auroral and geomagnetic activity led to the suggestion that the charged particles from the Sun impact and perturb the geomagnetic field almost continuously. Variations in the cosmic ray intensity,

measured on the surface of the Earth, were found to follow an  $\sim 11$  year cycle,  $180^\circ$  out of phase with the solar activity cycle. One possible explanation of this fact was that the magnetic fields embedded in plasma clouds emitted from the Sun during flares sweep away the cosmic rays from the interstellar space.

The first evidence for a continuous outflow of plasma from the Sun came from Biermann's observations of ionic comet tails in early 1950s. He noticed that the comet tails always point away from the Sun, independent of the orbital inclination, and offered an explanation in terms of an interaction between the material emitted from the comets and the plasma continuously moving away from the Sun. Biermann estimated a particle flux of  $\sim 10^9$  protons  $cm^{-2} s^{-1}$  at 1 AU, remarkably close to the modern day estimates from *in-situ* satellite observations at 1 AU of  $\sim 4 \times 10^8$  protons  $cm^{-2} s^{-1}$ .

### 1.4.2 Parker's model

On the theoretical front, most theories of solar atmosphere treated the corona as static and gravitationally bound till late 1950s. The main stumbling block for this model was that it required the pressures at very large distances from the Sun to be seven to eight orders of magnitude larger than the estimated pressure of the interstellar plasma. This mismatch in pressure at large heliocentric distances inspired Parker to reason that the solar corona could not be in static equilibrium and therefore must be expanding. In 1958 Parker presented his theoretical model for the Solar Wind which used hydrodynamic equations for conservation of mass, momentum and energy for a hot solar corona. Figure showing velocity evolution of the Solar Wind as a function of radial distance from the Sun is reproduced from his original work. His model gave a picture in which the velocity of the Solar Wind is low close to the Sun and becomes supersonic as it traverses away from the Sun and has vanishingly small pressure at large heliocentric distances. Parker coined the term *Solar Wind* to emphasise the fluid character of the solutions which describe the continuous supersonic coronal expansion. Firm observational evidence for existence of Solar Wind was presented by Snyder and Neugebauer by direct measurements using the plasma analyser onboard the Mariner-2 space probe in 1962.

## 1.5 Means of studying the Solar Wind

The Solar Wind has been studied using both direct sampling methods using space observatories and remote sensing techniques. Numerous satellites have been launched in order to study the physical properties of the Sun and the Solar Wind. The payloads on board these satellites perform a variety of different measurement and

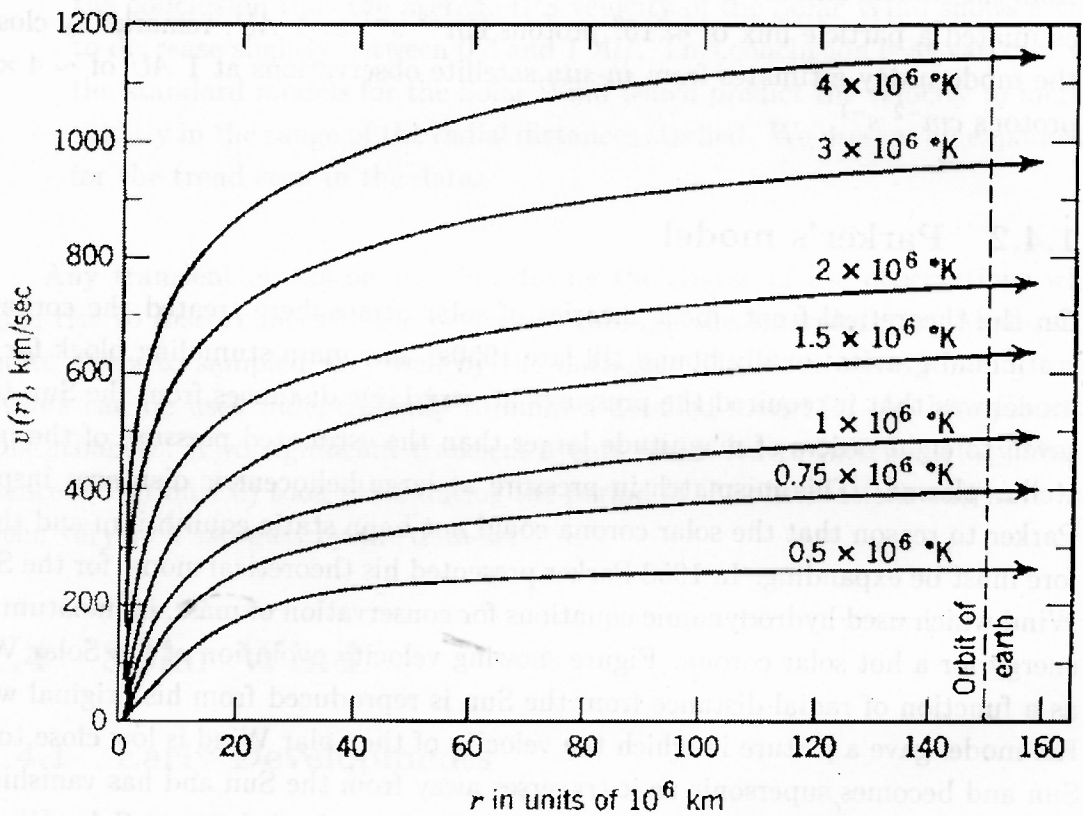


Figure 1.2: Speed of the Solar Wind with heliocentric distance – The figure shows Parker's original solutions for speed of the Solar Wind as a function of the heliocentric distance for different values of coronal temperatures. This figure has been reproduced from *Interplanetary Dynamical Processes*, 1963.

can be categorised broadly into plasma analysers and flux monitoring or imaging instruments. The plasma analysers perform *in-situ* measurements of the local Solar Wind plasma. They measure physical parameters like number density, velocity, temperature of electrons and protons and magnetic field orientation and magnitude. The other instruments monitor the flux of the Sun in various wavebands ranging from *UV* to hard *X* rays and image of the solar disc and the corona in a range of wavelengths from *UV* to hard *X* rays. Among the remote sensing tools, IPS is the most important and often used technique to study the Solar Wind.

Both, direct sampling and remote sensing observation techniques, used to study the Solar Wind, have their respective advantages and disadvantages. Direct sampling by satellites provides data which is much less dependent on the various assumptions which are crucial for interpreting the indirect observations. Satellites, on the other hand, provide only spot measurements of plasma parameters, which, in principle, cannot distinguish between temporal and spatial variations in a model independent manner. The vast expanse of the heliosphere is sampled very poorly by our existing set of satellites and their locations, relative to each other, are rarely suitable for investigating large scale structure in the Solar Wind. IPS, on the other hand, has the advantage that it has a large fraction of the inner heliosphere accessible to it any given time and IPS measurements are inherently sensitive to the distribution of Solar Wind properties along the entire *l.o.s.* IPS thus forms an ideal and low cost tool to investigate the large scale structure of the Solar Wind, which cannot be studied by any other existing means. As IPS is an indirect measurement technique, IPS observables can be related to Solar Wind parameters only in a model dependent manner. The current state of the knowledge about the Solar Wind constrains the values of some of the parameters of the IPS model for Solar Wind to lie in a small range, so the uncertainties in interpretation, due to the dependence on model parameters, is not large.

## 1.6 Properties of the Solar Wind

A large body of information has been gathered about the Solar Wind from both ground and space based observations since the discovery of Solar Wind in 1964. This section discusses some of the rather well established properties which are of relevance to this work and are often referred to in the following chapters. An excellent treatment of the subject is available in considerable detail along with a useful set of references in a set of two volumes edited by Schwenn and Marsch (Schwenn and Marsch, 1990a,b).

## General properties

Solar Wind has traditionally been thought of as being composed of two distinct components, a smooth and featureless ambient or quiescent component which is ubiquitous and has reasonably well known and stable large scale properties and a disturbed component which constitutes primarily of transients and is superposed on the ambient Solar Wind. Most of the discussion in this section relates to the ambient Solar Wind and especially to its properties close to the minima of the solar activity cycle. The simplest models of the Solar Wind assume the ambient medium to be a featureless steady outflow of magnetised coronal plasma. For such models the radial profiles for velocity and density of the plasma are well known. The acceleration region of the Solar Wind lies close to the Sun and most observations have found the Solar Wind to be already accelerated to its velocity at 1 AU by the time it reaches  $\sim 20 R_{\odot}$ . The Solar Wind velocity is almost purely radial, the non-radial components of the velocity are usually smaller than a few percent of the radial component. Beyond the acceleration region, the ambient Solar Wind plasma is believed to flow outwards with practically a constant velocity. As a consequence of the radial outflow with a constant velocity, the number density of the ambient Solar Wind plasma falls off as  $R^{-2}$ , where  $R$  is the heliocentric distance. It has now been established that the ambient wind is endowed with considerable structure and that its large scale properties change with the phase of the solar activity cycle. There is now a growing consensus that the ambient wind comprises of two distinct kinds of the Solar Wind, the slow wind and the fast wind which differ in their physical properties and sites and mechanisms of origin and can be clearly distinguished between by the present observations.

## Structure of Interplanetary Magnetic Field

The plasma comprising the Solar Wind is a very good electrical conductor. As the consequence, the solar magnetic field is *frozen* in the plasma. As the coronal plasma expands away, it carries along with it the solar magnetic field. The near radial motion of the Solar Wind and the rotation of the Sun cause the magnetic field lines to bend into spirals, in the plane of the solar equator. The pitch angle of the spiral is related to the angular speed of rotation of the Sun,  $\Omega_{\odot}$ <sup>2</sup> and the velocity of the Solar Wind,  $V_{SW}$ , by the relation :

$$d\theta = \Omega_{\odot} dt = \Omega_{\odot} \frac{dR}{V_{SW}} \quad (1.1)$$

where  $d\theta$  is the change in the azimuthal angle in time  $dt$  and  $dt$  is the time taken to travel a radial distance of  $dR$  with a constant radial velocity,  $V_{SW}$ . Such spi-

---

<sup>2</sup> $\Omega_{\odot} = 1.642 \times 10^{-4} \text{ deg sec}^{-1}$



rals, which turn through equal angles in equal radial distances, are referred to as *Archimedean spirals*. Figure 1.3 shows the structure of the magnetic field in the Interplanetary Medium in the solar equatorial plane, as seen from the solar North pole. A constant radial speed of  $400 \text{ km sec}^{-1}$  has been used to generate the spirals. The magnetic field lines of force are inclined at  $\sim 45^\circ$  to the radial direction from the Sun at 1 AU. The magnetic field lines trace out the locus of the plasma packets arising from a given fixed point on the solar surface, while the individual plasma packets themselves move radially outwards. The field lines outside the plane of the solar equator are also spirals wrapped around the solar rotation axis. This picture is in reasonable agreement with the observed average orientation of magnetic field at a range of heliocentric distances and latitudes, though the instantaneous values of the magnetic field undergo large deviations.

### Stream Structure

It was realised quite early, from the photographs of the solar corona taken at the times of solar eclipse, that the solar corona is highly structured and changes very significantly during the solar activity cycle. It is, therefore, reasonable to expect that this structure and time variability should also manifest itself in the Solar Wind which the corona expands into. While the Parker's model describes a featureless Solar Wind, the real Solar Wind is known to have considerable structure. In the ecliptic plane, the Solar Wind tends to be organised in alternating low and high velocity streams, especially close to the solar minima. The high speed streams originate in the *coronal holes*. Coronal holes are regions of large spatial extent in the solar atmosphere with practically unipolar field and are comparatively inactive regions of the solar surface. These regions appear dark in coronagraphs because the coronal density in them is rather low. The low density arises because the plasma in the coronal hole regions can expand with comparative ease by flowing along the field lines. The closed magnetic field lines, on the other hand, restrain the plasma from freely expanding away and the slow wind arises from above these more active regions of the Sun and shows much higher variability of all its properties. The high speed streams are therefore unipolar in nature while sharp long lived field reversals take place in the intervening slow speed wind streams.

### The Ballerina Skirt Model

The magnetic field of the Sun can be described by a dipolar magnetic field, to a first order. Close to the minima of solar activity cycles, the following scenario holds. The magnetic poles of the Sun are covered by large coronal holes, areas of open magnetic field lines. Some of the coronal holes migrate to low latitude regions, well into the equatorial regions. This is due to the fact the global solar dipole axis is

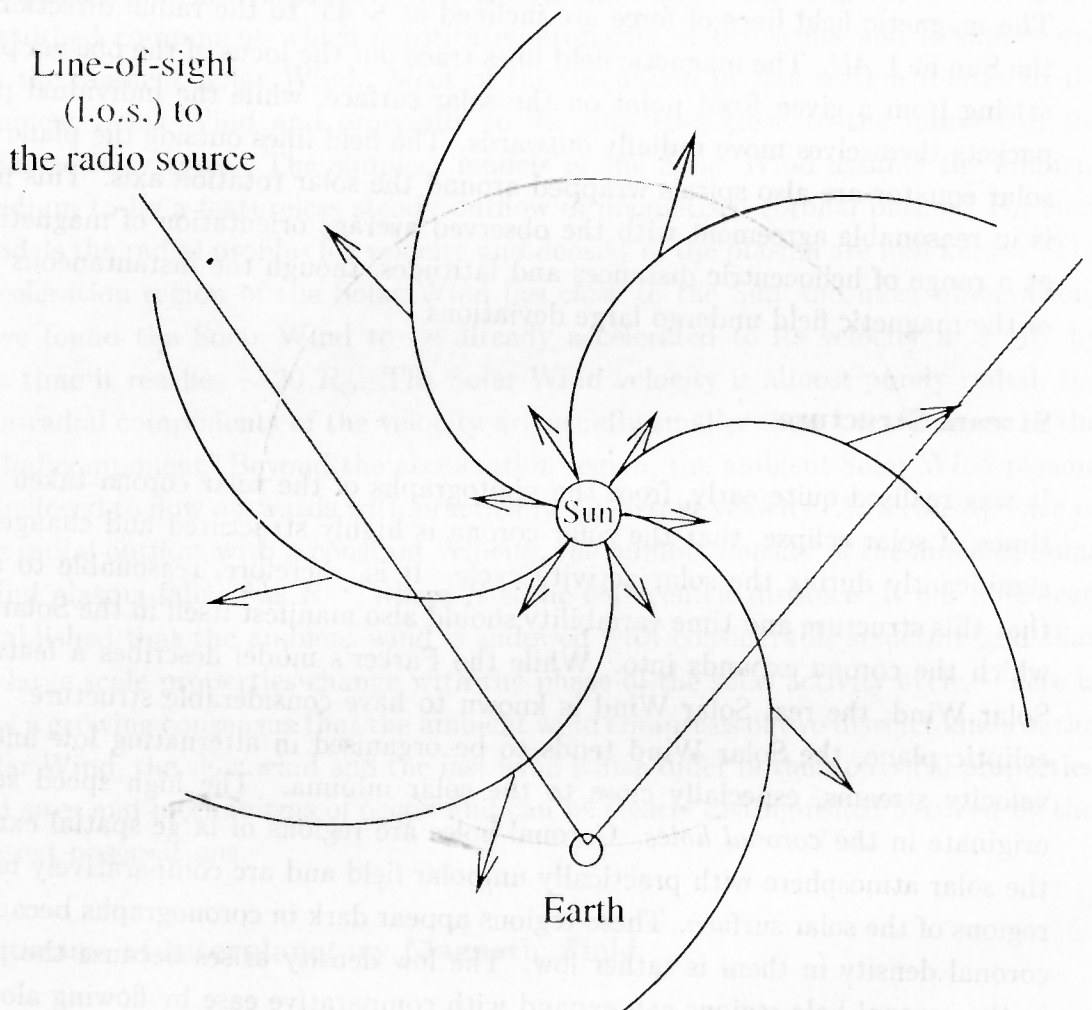


Figure 1.3: **Structure of the magnetic field in the Interplanetary Medium** – A view of the structure of the magnetic field in the solar equatorial plane, as seen from the North pole is shown. The velocity of the Solar Wind is assumed to be a constant and along the radial direction and is shown by the arrows. A velocity of  $400 \text{ km sec}^{-1}$  has been used to generate this figure. The radial velocity of the Solar Wind causes the magnetic field lines frozen in the plasma to bend into Archimedean spirals. For a velocity of  $400 \text{ km sec}^{-1}$ , the magnetic field lines make an angle of  $\sim 45^\circ$  with the radial direction from the Sun at 1 AU.

titled with respect to the solar rotation axis, though tilt is small at solar minima. The active regions, with their closed magnetic field configurations, are confined to the equatorial regions on the Sun. There is a thin boundary which separates the hemisphere with positive open field lines from the one with negative open field lines. This boundary takes the form of a sheet as the Solar Wind is convected away and is referred to as the *Heliospheric Current Sheet* (HCS). The warps in the HCS make it appear like the skirt of a twirling ballerina. This skirt is generally *attached* to the corona in the middle of the near-equator activity belt and in between the large coronal holes. This model, referred to as the *Ballerina Model* was first proposed by Alfven (Alfven, 1977). The undulations in the HCS, lead to the consequence that the magnetic field detected by the Earth orbiting satellites is organised into alternating regions of positive and negative polarities. The HCS is usually detected in the satellite plasma data as a region of high plasma density with long lived structures of opposite magnetic field polarities sandwiching it. This organisation of the magnetic field is referred to as sector structure of the Solar Wind and the size and the number of structures is closely related to the structure of the underlying corona.

### Latitudinal Structure

Historically, the first indication for the variation of Solar Wind properties with heliographic latitude came from IPS studies by Dennison and Hewish, in 1967, when they reported for the first time a trend for velocity of the Solar Wind to increase at high latitudes (Dennison and Hewish, 1967). Coles and Rickett presented convincing evidence, using IPS data, for an increase in the velocity of the Solar Wind out of the equatorial plane (Coles and Rickett, 1976). Many subsequent observations have now established the latitudinal structure of the Solar Wind on a firm footing (Kojima and Kakinuma, 1990; Ananthkrishnan et al., 1995).

In view of the fact that the embedded magnetic field in the Solar Wind can strongly influence its properties by channelling the coronal expansion (Hundhausen, 1972), many investigations were carried out to study the association of the Solar Wind structure with the *heliomagnetic*, rather than *heliographic*, latitude. In the current context, the term heliomagnetic latitude, denotes the local latitudinal separation from the warped HCS, the heliomagnetic equator. As the solar activity cycle progresses from a minima to a maxima, the angle between the heliomagnetic axis and the axis of rotation of the Sun increases. This leads to increasing warps of larger amplitudes in the HCS and causes the sector structure to extend to much higher latitudes. Most of these studies exploited these warps in the HCS to sample a substantial range of heliomagnetic latitudes using spacecrafts confined to the ecliptic. Many such studies were compared by Bruno (Bruno et al., 1986) and all of them had the common characteristic that the *slow* Solar Wind is found in a belt with a

width of about  $\pm 20^\circ$  around the heliomagnetic equator and only *high* speed wind is found outside this region. Kojima and Kakinuma (Kojima and Kakinuma, 1990) also arrive at a similar conclusion using IPS data. Close to the solar minima, the heliomagnetic equator is close to the heliographic equator, hence heliomagnetic and heliographic latitudes do not differ much from each other.

### Co-rotating Interaction Regions

As has been mentioned before, close to the minimum of the solar activity cycle, some of the coronal holes migrate down to the equatorial belt. These coronal holes are often stable over time scales of many solar rotations<sup>3</sup> and lead to the high and low speed streams described earlier. When the coronal expansion is spatially variable but time stationary, steady flow patterns develop in the equatorial plane, due to interaction of the slow and the fast Solar Wind. These long lived patterns co-rotates with the Sun.

The curvature of the flux tubes is inversely proportional to the velocity of the plasma contained in the flux tube (equation 1.1). The flux tubes with plasma at higher velocities are less tightly wound than the ones with plasma at slower velocities, their angular separation, therefore, changes as they propagate radially outwards. To provide a feel for the magnitude of this effect, the separation between Archimedean spirals followed by two streams with velocities 300 and 600  $km\ sec^{-1}$ , respectively, changes by  $41^\circ$  as they travel from the solar surface to 1 *AU*. The rotation of the Sun, therefore, causes the Archimedean flux tubes containing plasma at a higher velocity to collide and interact with slower plasma ahead of it, as shown in Figure 1.4. As the fast moving Solar Wind tries to overtake the slower plasma ahead of it and moves away from the slower plasma behind it, the structure of Solar Wind along the longitude, its longitude profile, changes as the wind moves outwards. The fast wind cannot stream through the slow wind because the two are threaded by different magnetic field lines which are frozen in them. The longitude profile of velocity evolves towards a rapid rise and slow decay shape, this is referred to as *steepening* of the velocity profile of the wind. The plasma on the rising part of the high speed stream has high density and is compressed and the plasma on the slow decay part of the high speed stream has a lower density than the ambient Solar Wind. The difference in velocity of the plasma in different flux tubes, thus, leads to the development of regions of compression and rarefaction, of both the plasma and the magnetic field. The compression regions in such a pattern are referred to as *Co-rotating Interaction Regions* (CIRs).

In presence of compressions and rarefactions the number density evolution of the Solar Wind streams differs significantly from the  $R^{-2}$  dependence, expected

<sup>3</sup>One solar rotation period is  $\sim 27$  days and is also referred to as *Carrington period*

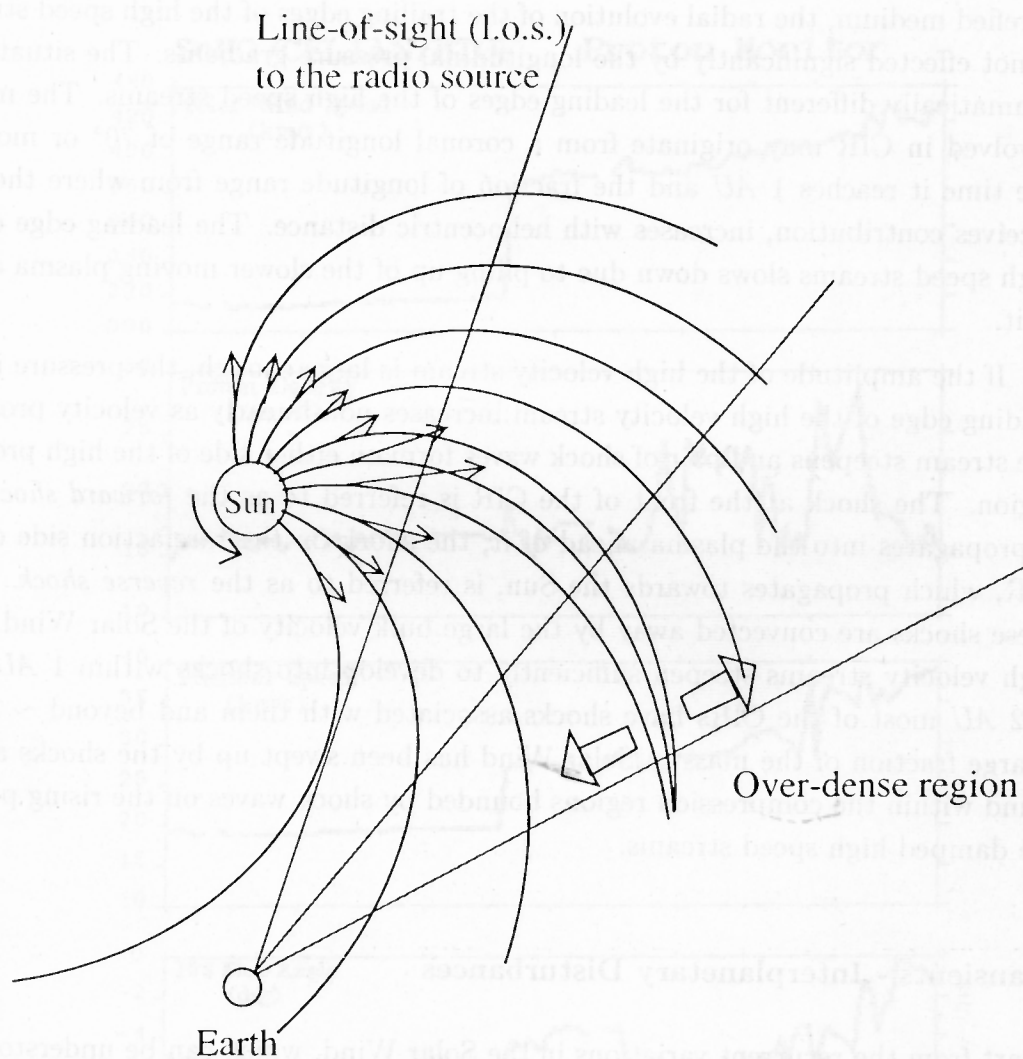


Figure 1.4: **Formation of Co-rotating Interaction Regions** – The figure illustrates, schematically, the scenario which leads to formation of quasi-stationary Co-rotating Interaction Regions (CIRs) in the plane of the ecliptic. The curves represent the Archimedean spirals which the magnetic field lines get bent into and the arrows the magnitude of the radial velocity vector. The sense of rotation of the Sun is also marked. The higher velocity streams push against the slower moving plasma ahead of it and lead to the formation of compression regions. The excess pressure in these over-dense regions leads to development of pressure gradients which impart non-radial velocities to the Solar Wind plasma. The figure also shows the Earth with a few *l.o.s.* to distant sources passing through the CIRs.

from spherical symmetry, and longitudinal pressure gradients also develop. These pressure gradients tend to fill in the rarefaction regions and also impart non radial velocities to the plasma on either side of the CIRs. As interaction is not significant in rarefied medium, the radial evolution of the trailing edges of the high speed streams is not effected significantly by the longitudinal pressure gradients. The situation is dramatically different for the leading edges of the high speed streams. The matter involved in CIR may originate from a coronal longitude range of  $70^\circ$  or more by the time it reaches  $1 AU$  and the fraction of longitude range from where the CIR receives contribution, increases with heliocentric distance. The leading edge of the high speed streams slows down due to piling up of the slower moving plasma ahead of it.

If the amplitude of the high velocity stream is large enough, the pressure in the leading edge of the high velocity stream increases non-linearly as velocity profile of the stream steepens and pair of shock waves form on either side of the high pressure region. The shock at the front of the CIR is referred to as the *forward shock* and it propagates into the plasma ahead of it, the shock on the rarefaction side of the CIR, which propagates towards the Sun, is referred to as the *reverse shock*. Both these shocks are convected away by the large bulk velocity of the Solar Wind. Few high velocity streams steepen sufficiently to develop into shocks within  $1 AU$ . By  $\sim 2 AU$  most of the CIRs have shocks associated with them and beyond  $\sim 5 AU$  a large fraction of the mass in Solar Wind has been swept up by the shocks and is found within the compression regions bounded by shock waves on the rising part of the damped high speed streams.

### Transients - Interplanetary Disturbances

Apart from the recurrent variations in the Solar Wind, which can be understood in terms of spatial variations in the co-rotating structures, there are sporadic disturbances which involve true temporal variations. These are referred to as *Interplanetary Disturbances* (IPDs). The most striking of these are the Interplanetary shock waves which propagate outwards from the Sun. Such a shock is seen by an observer as an abrupt change in the values of the physical properties of the Solar Wind like speed, density, temperature and the strength and orientation of the magnetic field. The change in the values of the physical properties persist for time scales of many hours after the shock front has passed through, at  $1 AU$ . An example of such a shock, from the period of observations presented in this work, is shown in Figure 1.5. It is now believed shock waves with thickness much smaller than the collision length scales can form in magnetised plasma of the Solar Wind, such shocks have been given the name *Collisionless shocks*. A shock front moving outwards through the Solar Wind overtakes the slow wind ahead of it and accelerates and heats up the

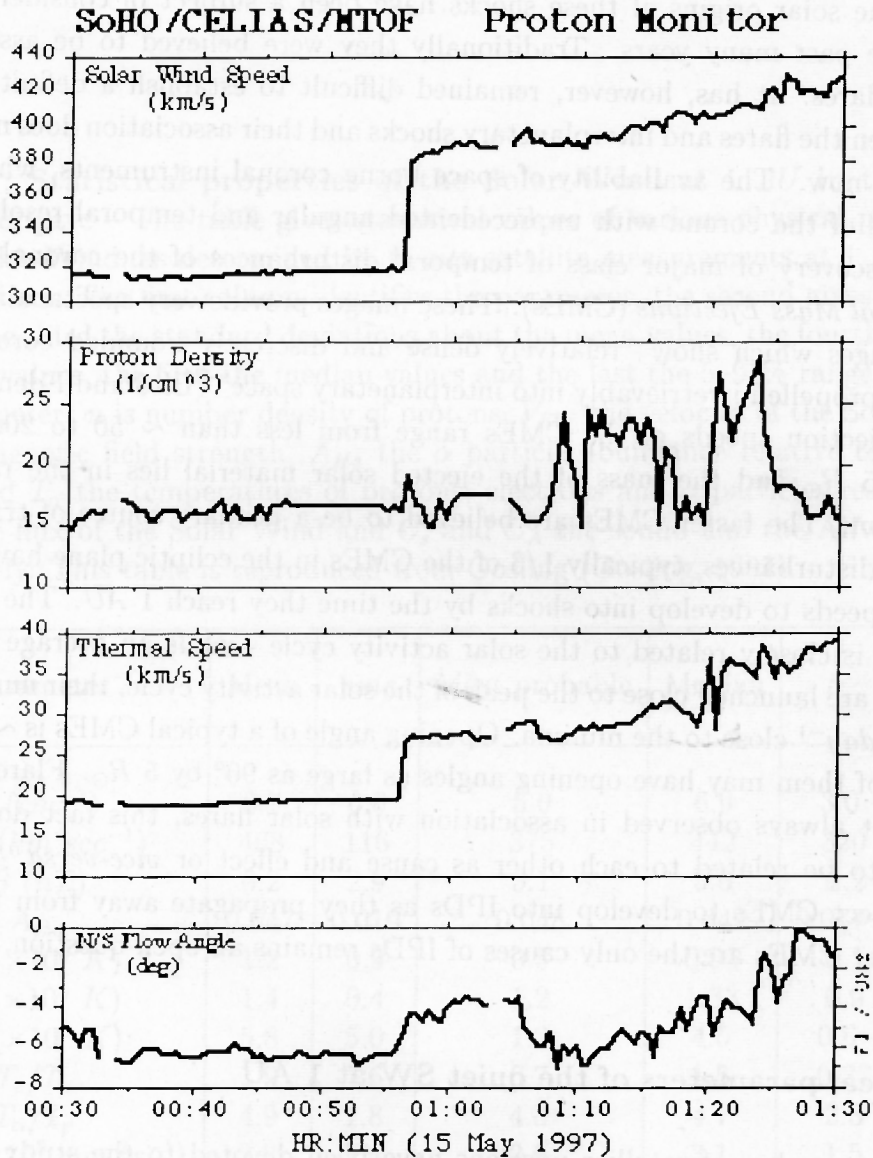


Figure 1.5: An Interplanetary Disturbance, as seen in Solar Wind plasma at 1 AU – The figure shows the time series of Solar Wind speed, proton density, thermal speed and  $N/S$  flow angle seen by the CELIAS/MTOF instrument onboard the SOHO satellite. This event has been identified to be an Earth directed Coronal Mass Ejection which was launched from the Sun on the 12<sup>th</sup> May 1997 and was seen at 1 AU on the 15<sup>th</sup> of May 1997.

material which passes through it. The shock thus transfers energy and momentum to the Solar Wind *shocked* medium. Unless the momentum and the energy of the shock are continually replenished, the shock must decelerate as it moves outwards.

The solar origins of these shocks have been a subject of considerable interest for the past many years. Traditionally they were believed to be associated with solar flares. It has, however, remained difficult to establish a definite connection between the flares and interplanetary shocks and their association does not find much favour now. The availability of space borne coronal instruments, which provided images of the corona with unprecedented angular and temporal resolution, led to the discovery of major class of temporal disturbances of the coronal plasma, the *Coronal Mass Ejections* (CMEs). These images provide very spectacular time-series of images which show “relatively dense and discretely bounded coronal material being propelled irretrievably into interplanetary space” (Bird and Edenhofer, 1990). The ejection speeds of the CMEs range from less than  $\sim 50$  to  $2000 \text{ km sec}^{-1}$  at  $\sim 5 R_{\odot}$  and the mass of the ejected solar material lies in the range  $10^{15}$  to  $10^{16} \text{ gm}$ . The faster CMEs are believed to be a primary source of transient Solar Wind disturbances, typically 1/3 of the CMEs in the ecliptic plane have sufficiently high speeds to develop into shocks by the time they reach 1 *AU*. The frequency of CMEs is closely related to the solar activity cycle - while an average of  $3.5 \text{ day}^{-1}$  CMEs are launched close to the peak of the solar activity cycle, their number reduces to  $0.5 \text{ day}^{-1}$  close to the minima. Opening angle of a typical CMEs is  $\sim 45^{\circ}$ , though some of them may have opening angles as large as  $90^{\circ}$  by  $5 R_{\odot}$ . Flares and CMEs are not always observed in association with solar flares, this fact does not allow them to be related to each other as cause and effect or *vice-versa*. It is natural to expect CMEs to develop into IPDs as they propagate away from the Sun, but whether CMEs are the only causes of IPDs remains an open question.

### Physical parameters of the quiet SW at 1 AU

A large number of satellite missions have been devoted to the study of the Solar Wind, since early 1960s. An overwhelming majority of these satellites are Earth orbiting and therefore sample the Solar Wind only in the ecliptic plane and at 1 *AU*. Over the past many years a vast database of measurements of physical properties of Solar Wind has been generated using the plasma analysers on-board these satellites. The statistical properties of the Solar Wind at 1 *AU* derived from these measurements in the ecliptic plane are listed in Table 1.1. This table is reproduced from Gosling (Gosling, 1997). The table includes the mean values, standard deviations about the mean values, most probable values, median values and the 5–95% range limits for the parameters. The parameters listed are number density of protons ( $n$ ), the velocity of the Solar Wind ( $V_{SW}$ ), the magnetic field strength ( $B$ ), the  $\alpha$  particle



Table 1.1: **Statistical properties of the Solar Wind at 1 AU in the plane of the ecliptic** – The table gives statistical values of various physical parameters of the Solar Wind, as determined by *in-situ* satellite measurements at 1 AU in the ecliptic plane. The first column identifies the parameter, the second gives the mean values, the third the standard deviations about the mean values, the fourth the most probable values, the fifth the median values and the last the 5–95% range limits for the parameter.  $n$  is number density of protons,  $V_{SW}$  the velocity of the Solar Wind,  $B$  the magnetic field strength,  $A_{He}$  the  $\alpha$  particle abundance relative to protons,  $T_p$ ,  $T_e$  and  $T_\alpha$  the temperatures of protons, electrons and  $\alpha$  particles respectively,  $nS_{SW}$  the flux of the Solar Wind and  $C_s$  and  $C_A$  the sound and the Alfvén speeds respectively. This table is reproduced from Gosling (Gosling, 1997).

Parameter	Mean	<i>rms</i>	Most probable	Median	5 – 95 %
$n$ ( $cm^{-3}$ )	8.7	6.6	5.0	6.9	3.0 – 20.0
$V_{SW}$ ( $km\ sec^{-1}$ )	468	116	375	442	320 – 710
$B$ ( $nT$ )	6.2	2.9	5.1	5.6	2.2 – 9.9
$A_{He}$	0.047	0.019	0.048	0.047	0.017 – 0.078
$T_p$ ( $\times 10^5$ K)	1.2	0.9	0.5	0.95	0.1 – 3.0
$T_e$ ( $\times 10^5$ K)	1.4	0.4	1.2	1.33	0.9 – 2.0
$T_\alpha$ ( $\times 10^5$ K)	5.8	5.0	1.2	4.5	0.6 – 15.5
$T_e/T_p$	1.9	1.6	0.7	1.5	0.37 – 5.0
$T_\alpha/T_p$	4.9	1.8	4.8	4.7	2.3 – 7.5
$nV_{SW}$ ( $\times 10^8\ cm^{-2}s^{-1}$ )	3.8	2.4	2.6	3.1	1.5 – 7.8
$C_s$ ( $km\ sec^{-1}$ )	63	15	59	61	41 – 91
$C_A$ ( $km\ sec^{-1}$ )	50	24	50	46	30 – 100

abundance relative to protons ( $A_{He}$ ), the temperatures of protons, electrons and  $\alpha$  particles ( $T_p$ ,  $T_e$  and  $T_\alpha$ ), the flux of the Solar Wind ( $nV_{SW}$ ) and  $C_s$  and  $C_A$  the sound and the Alfvén speeds ( $C_s$  and  $C_A$ ). As is evident from this table, the Solar Wind parameters vary over a considerable range. The speed of the Solar Wind is much larger than sound speed and Alfvén speed at 1 AU, the flow is thus both supersonic and superalfvénic. It is also interesting to note the average values of  $T_e$ ,  $T_p$  and  $T_\alpha$  are not equal.

## 1.7 Organisation of the thesis

The thesis is organised in eight chapters, the basic thrust of each of them is briefly described below.

The present chapter introduces the technique of IPS and offers a very brief historic account of the development of the subject. This chapter also presents the motivation for the present work, introduces the Solar Wind and describes a few established properties of the Solar Wind of relevance to this work.

The second chapter discusses the theory of IPS. The emphasis has been on presenting the final frame work of the formulation used and discussing it in some depth rather than developing the formalism. The formalism is justified using physical arguments rather than mathematical rigour. The assumptions relied upon and their domains of validity are clearly highlighted. The effects of each of the parameters of the Solar Wind model on the observed power spectra are also discussed.

The third chapter begins with a discussion of the estimation of the properties of the Solar Wind from single station studies of IPS, the applications they have been used for and their limitations. It goes on to point out violations of the assumptions made by these models in the actual Solar Wind scenarios. The formulation of the problem of tomography is presented and the basic requirements for an observable to be useful for a tomographic reconstruction are discussed. The feasibility of using IPS data for a tomographic reconstruction of the Solar Wind in the inner heliosphere is discussed. The data, software and computing requirements for such an exercise are estimated. The advantages and limitations of such a reconstruction are presented.

The fourth chapter describes the data-set which was obtained to attempt a tomographic reconstruction of the Solar Wind. The criterion for source selection and the coverage of inner heliosphere achieved by the data-set are discussed. The data processing carried out to compute the basic IPS observables, the scintillation index and the power spectra of intensity fluctuations is described along with computation of their respective statistical uncertainties. Computation of  $g$  values is also described.

Chapter five discusses the automated procedure developed to estimate the best fit IPS model for the observed power spectra. This procedure is basically a  $\chi^2$  minimisation procedure with the  $\chi^2$  defined in an appropriate manner. The criterion which a suitable definition of the  $\chi^2$  must satisfy are presented. Our implementation of the procedure is discussed in considerable detail. The extensive simulations carried out to validate the automated procedure and their results are described. The results of using the procedure on the observed data are shown and a discussion on their interpretation is presented. The reliability of the automated procedure is clearly established by presenting a large number of power spectra which provide a fair sample of the observed data-set. A glimpse of the observed data-set is provided in the form of time series of IPS parameters estimated for individual sources.

The sixth chapter describes our results regarding the radial evolution of the Solar Wind. We see a significant trend for decrease in the average IPS velocity of the equatorial Solar Wind as it travels outwards. The observed decrease in the average velocity with radial distance is critically examined. It is shown that the trend is a genuine feature of the data-set and is not an artifact of the analysis procedure or the sampling of the heliosphere. Our interpretation of this result is also presented.

Chapter seven discusses our formulation of the problem of tomographic reconstruction and highlights the differences from and improvements over the previous attempts. The large set of simulation done to validate both the software and the methodology developed are presented. The results of the simulations which established the efficacy the both the software and our procedure are discussed in detail. The results of application of the methodology to the observed data-set are presented and some comparisons with other independent data-sets are made. The conclusions drawn from these results and their implications are discussed in depth.

The final chapter summarises the conclusions arrived at in this work and makes some comments on the utility of tomography as a routine investigation tool for the Solar Wind.

Chapter five discusses the numerical procedure developed to estimate the best fit model for the observed power spectra. The procedure is based on a minimum variance procedure with the  $\chi^2$  defined in an appropriate manner. The optimization which a suitable definition of the  $\chi^2$  must satisfy are presented. Our implementation of the procedure is described in considerable detail. The essential operations carried out to validate the automated procedure and their results are described. The results of using the procedure on the observed data are shown and a discussion on their interpretation is presented. The reliability of the automated procedure is clearly established by presenting a large number of power spectra which provide a fair sample of the observed data set. A glimpse of the observed data set is provided in the form of time series of IPS parameters estimated for individual sources.

The sixth chapter describes our results regarding the radial evolution of the Solar Wind. We see a significant trend for decrease in the average IPS velocity of the equatorial Solar Wind as it travels outwards. The observed decrease in the average velocity with radial distance is briefly explained. It is shown that the trend is a genuine feature of the data set and is not an artifact of the analysis procedure or the sampling of the heliosphere. Our interpretation of this result is also presented.

Chapter seven discusses our formulation of the problem of tomographic reconstruction and highlights the differences from and improvements over the previous attempts. The large set of simulation done to validate both the software and the methodology developed are presented. The results of the simulations which are labeled in this way, the both the software and our procedure are discussed in detail. The results of application of the methodology to the observed data set are presented and some comparisons with other independent data sets are discussed. The results of tomographic reconstruction and their implications are discussed in detail.

The final chapter summarizes the conclusions arrived at in this work and makes some comments on the utility of tomography as a routine investigation tool for the Solar Wind. The conclusions are summarized in a separate section to make the book more self-contained. The feasibility of a non-destructive solar wind tomography is discussed in the inner heliosphere. The data, software and computing requirements are discussed. The advantages and limitations of such a reconstruction are presented.

The fourth chapter describes the data set which was obtained to attempt a tomographic reconstruction of the Solar Wind. The criteria for source selection and the coverage of the heliosphere achieved by the data set are discussed. The data processing carried out to compute the basic IPS observables, the scintillation index and the power spectra is described in considerable detail. The data set is also described.